

5

CONFOCAL MICROSCOPY OF SKIN CANCER

JULIANA CASAGRANDE TAVOLONI BRAGA

Hospital A. C. Camargo, São Paulo, Brazil

ITAY KLAZ AND ALON SCOPE

Memorial Sloan–Kettering Cancer Center, New York, New York

DANIEL GAREAU

Oregon Health and Science University, Portland, Oregon

MILIND RAJADHYAKSHA AND ASHFAQ A. MARGHOOB

Memorial Sloan–Kettering Cancer Center, New York, New York

5.1	Introduction	164
5.2	Imaging of normal skin in vivo	166
5.2.1	Epidermis	166
5.2.2	Dermal–epidermal junction	166
5.2.3	Dermis	167
5.3	Imaging of cutaneous neoplasms in vivo: correlation with dermoscopy and histopathology	168
5.3.1	Basal cell carcinoma	168
5.3.2	Actinic keratosis and squamous cell carcinoma	170
5.3.3	Melanoma	171
5.4	Mosaicing of excised skin ex vivo	174
5.5	Intraoperative mapping of surgical margins	177
5.6	Challenging cases	177
5.7	Future perspectives	182
	References	183

Advances in Optical Imaging for Clinical Medicine, Edited by Nicusor Iftimia, William R. Brugge, and Daniel X. Hammer
Copyright © 2010 John Wiley & Sons, Inc.

5.1 INTRODUCTION

Although Marvin Minsky invented the confocal microscope in 1957, the instrumentation and applications for the *in vivo* evaluation, diagnosis, and management of cutaneous tumors has only evolved during the past decade. Reflectance confocal microscopy (RCM) consists of a point source of light, produced by a laser beam, which passes through an objective lens and illuminates a probe volume in skin. The light backscattered from the probe volume passes through an optically conjugate point aperture, consisting of a pinhole, and is then captured by a detector to produce a pixel. Scanning the probe volume in two dimensions permits the operator to capture a corresponding two-dimensional array of pixels, which produces an image of a thin optical section within thick tissue. Imaging of thin optical sections is noninvasive, in contrast to conventional histology, which requires physical sectioning of tissue.

RCM enables real-time visualization of nuclear and cellular morphology *in vivo*. The ability to observe nuclear and cellular details clearly sets this imaging modality apart from other noninvasive imaging instruments, such as magnetic resonance imaging [1], optical coherence tomography [2], and high-frequency ultrasound [3]. The lateral resolution of RCM is typically 0.2 to 1.0 μm , and the thickness of optical sectioning is 1 to 3 μm [4,5], which is analogous to viewing histology at high magnification power and high resolution. As a result, RCM is being developed as a portable bedside tool for diagnosis of melanoma [6] and nonmelanoma [7] skin cancers.

At present, there is a commercially available reflectance confocal microscope (VivaScope 1500, Lucid Inc., Rochester, New York), consisting of a scanning unit that is mounted on an articulating arm for positioning on the patient. A metal ring fixture with an adhesive window is applied to the skin. The microscope is then coupled to the metal ring, thereby creating a stable contact between the skin and the objective lens. A gel with a refractive index close to that of water (i.e., 1.33) is placed between the objective lens and the tissue. With a $30\times$ lens, the field of view in the tissue is 0.5×0.5 mm. However, larger fields of view are achievable by “stitching” together, via computer software, sequentially acquired adjacent images to create and display a mosaic. The current version of this software allows up to 16×16 images to be “stitched” together, thereby creating and displaying up to an 8×8 mm field of view. This is analogous to a low magnifying power of $2\times$. Imaging more than 16×16 images is currently impractical, due to the long acquisition times required for imaging such a large field. Use of a near-infrared wavelength of 830 nm permits imaging to depths of 100 to 200 μm in normal skin. This allows for visualization of the epidermis and superficial dermis. Although 830 nm is the wavelength of choice for most clinical applications, longer wavelengths such as 1064 nm, as well as shorter visible wavelengths of 488 to 700 nm, have been used. While shorter wavelengths provide higher resolution and thinner optical sectioning, longer near-infrared wavelengths allow deeper imaging, due to reduced scattering.

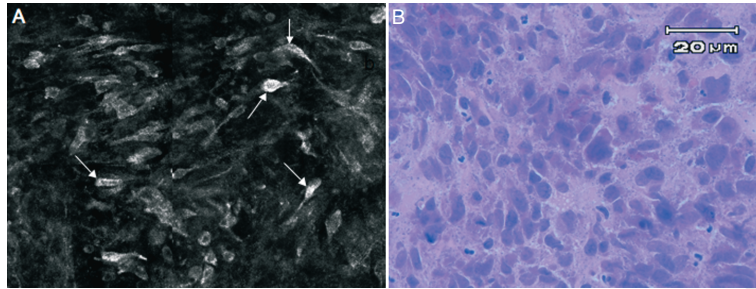


Figure 5.1 (A) RCM image of skin and (B) corresponding histology. Melanocytes appear in the black-and-white RCM images as bright cells against a dark background. The roundish dark structures within the outline of some of the cells correspond to the nucleus. In contrast, melanocytes in the corresponding H&E-stained histopathology section show purple nuclei and pink cytoplasm on a light pink background. The melanocytes shown are those of a melanoma; they are abnormal because they display variability in the size, shape, and refractivity of cells on RCM and variability in the size and shape of nuclei on H&E histopathology. The scale pertains to both images.

Although RCM is able to image at a resolution comparable to histology, there are some important differences between RCM and conventional histopathology. First, RCM images appear in black and white as opposed to the purple and pink colors seen in hematoxylin and eosin (H&E)-stained histology. Second, there is a contrast inversion with RCM. In routine histological staining with H&E, structures that absorb the stain appear dark in contrast to the nonstained bright background (Figure 5.1). In other words, H&E histology represents bright-field imaging. However, in RCM, the background tissue appears dark, while cells with higher reflectance appear brighter (Figure 5.1). This is equivalent to dark-field imaging. Third, although the nominal resolution and optical sectioning of RCM is similar to that of histopathology, the RCM image quality degrades with increasing depth in the tissue. At deeper dermis levels, strong scattering and aberrations at the dermal-epidermal junction (DEJ) and superficial dermis cause loss of optical sectioning, loss of resolution, and loss of contrast. Since structure-specific stains are not being applied *in vivo* to living human skin, we must rely solely on endogenous reflectance contrast for imaging. Unfortunately, image quality does degrade with loss of endogenous contrast. By comparison, observation of physically prepared thin histopathologic sections is superior to RCM images obtained *in vivo* because there is no overlying tissue to degrade the image and because of the benefit of stains to enhance contrasts. This fact, in turn, explains the reason for why *ex vivo* RCM imaging of tissue can produce an image quality that closely approaches that of histopathology.

Melanin provides the best source of endogenous contrast by strongly backscattering light. Cells that contain melanin, including melanocytes (Figure 5.1), keratinocytes, and dermal melanophages, appear bright on RCM. In general, the greater the melanin content and concentration within cells, the brighter the RCM images will appear. Some organelles and cytoplasmic granules, such as

keratohyaline granules in keratinocytes and Birbeck granules in Langerhans cells, also provide contrast, thus allowing them to be visualized as well [5].

5.2 IMAGING OF NORMAL SKIN IN VIVO

An essential component of recognizing cutaneous pathology via RCM is the ability to first recognize the features of normal skin. RCM images thin optical sections of tissue in the *en face* (horizontal) plane, allowing for evaluation of each of the different layers of epidermis, as well as the DEJ and superficial dermis. The normal skin appearance with RCM varies according to skin color, anatomical site, sun exposure, age, and physiological condition [8].

5.2.1 Epidermis

The epidermis is composed primarily of keratinocytes, which are arranged in four layers: stratum corneum, granular layer, spinous layer, and basal layer. In addition to keratinocytes, few melanocytes and Langerhans cells can also be seen occasionally. Each epidermal layer has specific features on RCM. The most superficial layer, the stratum corneum (Figure 5.2A), is located 0 to 15 μm from the skin surface and composed of flat anucleated keratinocytes (25 to 50 μm in size). The keratinocytes appear as groups of bright cells separated by dark, nonreflective skin folds or dermatoglyphics [5,8,9]. The second layer from the surface is the stratum granulosum (Figure 5.2B), located 10 to 20 μm from the skin surface; it is two to four cells in thickness and composed of polygonal cells (25 to 35 μm in size). Next is the stratum spinosum (Figure 5.2C), located 20 to 100 μm under the stratum corneum and also containing polygonal keratinocytes (15 to 25 μm in size). Individual keratinocytes of the granular and spinous layers are recognized by their outline of roundish dark center and surrounding bright ring, corresponding to nucleus and cytoplasm, respectively. This outline is probably due to the fact that native chromatin in the nucleus scatters much less light than keratin in the surrounding cytoplasm. Aside from the size difference, the refractive cytoplasm of keratinocytes of the stratum granulosum appears on RCM brighter and more granular than that of the stratum spinosum keratinocytes. The back-to-back arrangement of the polygonal keratinocytes in these two layers forms a pattern on RCM that resembles a honeycomb (Figure 5.2B and C). The basal layer of the epidermis is located 40 to 130 μm below the skin surface. It consists of a single layer of keratinocytes (7 to 12 μm in size), with episodic intervening melanocytes. The keratinocytes are usually uniform in shape and size and appear brighter than those in the spinous layer [5,8,9], forming a pattern that resembles a cobblestone (Figure 5.2D). The brightness of the basal keratinocytes is due to melanin that accumulates over the nucleus like a cap.

5.2.2 Dermal–Epidermal Junction

At this level the dermis forms upward fingerlike projections into the epidermis called *dermal papillae*. They appear on RCM images as round dark areas, often

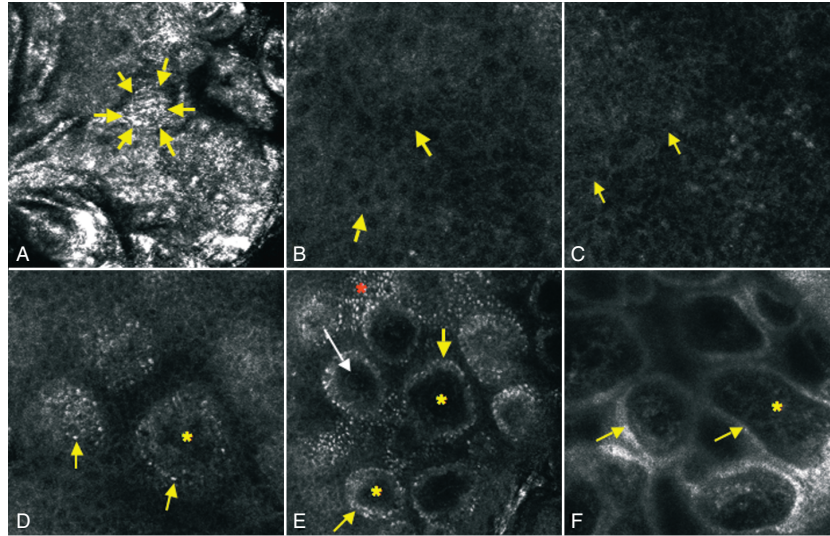


Figure 5.2 RCM images (0.5×0.5 mm) of normal skin. (A) The stratum corneum appears as highly refractile surface with dark skin folds. The cells appear to blend together because of poorly demarcated cell borders (arrows). (B) Stratum granulosum shows a honeycomb pattern made of polygonal keratinocytes with grainy cytoplasm and dark central nuclei (arrows). (C) Stratum spinosum also shows a honeycomb pattern; spinous keratinocytes are smaller, but otherwise also show a dark central nucleus surrounded by a rim of bright cytoplasm (arrows). (D) The basal layer consists of a pattern resembling cobblestone, formed by clusters of small bright basal keratinocytes (arrows). The dark area in the center of one of these clusters is a dermal papillae (asterisk). (E) The DEJ consists of rings of bright basal keratinocytes (yellow arrows) surrounding dark dermal papillae (yellow asterisks). A cobblestone pattern is seen (red asterisk), indicating that these cells are probably basal keratinocytes. Curved dark canalicular structures, corresponding to capillary loops, are also seen in the dermal papillae (white arrow). (F) In the dermal papillae, a network of reticulated gray fibers (asterisk) is seen around the central capillary. The dermal papillae are surrounded by bright rings of basal keratinocytes (arrows).

containing a central vascular lumen (papillary dermal vascular loops) that displays blood flow in real-time imaging. The dark dermal papillae are surrounded by a ring of bright keratinocytes of the epidermal basal layer (Figure 5.2E). In dark-skinned persons the rings formed by pigmented basal keratinocytes are brighter and more discernible than in light-skinned people, because basal keratinocytes in dark-skinned people contain more melanin [9].

5.2.3 Dermis

The dermis is located below the DEJ and varies, in thickness from 0.3 to 3.0 mm, depending on the anatomical site (e.g., relatively thin on the face and thick on the back). The dermis consists of blood vessels, nerves, inflammatory cells,

and fibroblasts enveloped in a network of collagen and elastic fibers. The dermis is divided into two regions, papillary and reticular dermis. The papillary dermis is located 50 to 150 μm beneath the skin surface and appears, on RCM, as thin intersecting collagen fibers. Where the DEJ is undulating (due to a pattern of alternating epidermal rete ridges and dermal papillae), the papillary dermis appears, as noted above, as round dark spaces surrounded by bright rings of basal keratinocytes (Figure 5.2F). In a flat DEJ, as seen in sun-damaged skin of the face, this pattern of bright rings around dermal papillae is usually absent. The reticular dermis is located more than 150 μm below the skin surface and only its upper portion can sometimes be visualized. Thicker collagen arranged in bundles is the main RCM feature of the reticular dermis.

Skin appendages such as eccrine ducts and follicular-sebaceous units can also be seen on RCM. Eccrine ducts appear as bright round structures that spiral through the epidermis. The hair follicles appears as a hollow structure whose wall is composed of elliptical keratinocytes and whose center lumen displays a highly reflective hair shaft [5,8,9].

5.3 IMAGING OF CUTANEOUS NEOPLASMS IN VIVO: CORRELATION WITH DERMOSCOPY AND HISTOPATHOLOGY

In the past two decades, new imaging tools have become available to clinicians who screen patients for skin cancer. Dermoscopy (also known as dermatoscopy and epiluminescence microscopy) is a very important skin screening tool that has been used increasingly over the past 15 years. A dermoscope is a hand-held tool that appears similar to an otoscope; dermoscopy allows the clinician to see structures of skin beneath the stratum corneum (which is normally not translucent), down to the depth of the superficial dermis, at a magnification of up to $10\times$. Many structures of skin seen on dermoscopy can be correlated with findings on histopathology, allowing the clinician using dermoscopy to make inferences about tissue pathology in vivo, prior to the actual biopsy. To this end, RCM has further enhanced our ability to assess skin cancer at the bedside, since RCM correlates well with both dermoscopy and histopathology. The fact that like dermoscopy, RCM images tissue in the horizontal plane (different from conventional histopathology, which views skin sections at the vertical plane) while having high magnification with cell-level resolution akin to histopathology makes RCM a bridge to correlation between dermoscopy and histopathology.

The use of RCM in the evaluation of skin cancers represents an important area of clinical research. Key RCM features of different cutaneous neoplasms have been described in the literature [9].

5.3.1 Basal Cell Carcinoma

Basal cell carcinoma (BCC) is the most common skin cancer in humans (Figure 5.3A and 5.3B) [10,11]. Histopathologically, BCCs are composed of

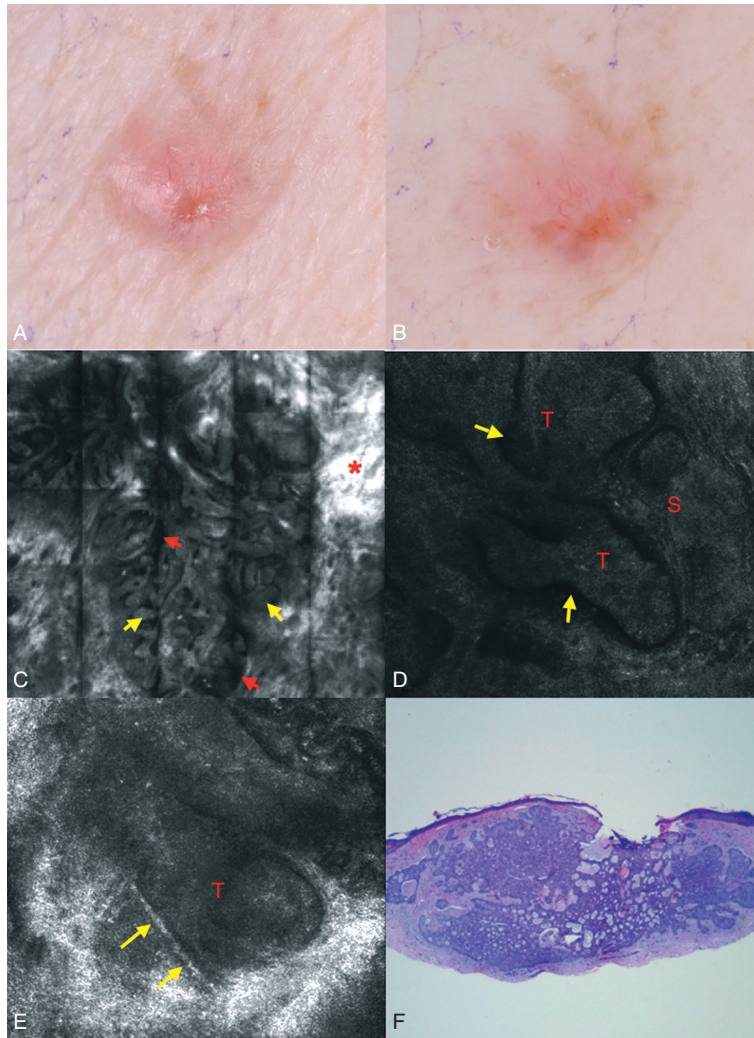


Figure 5.3 (A) Clinical photograph of an erythematous shiny papule on the upper arm. (B) On dermoscopy the lesion shows features suggestive of BCC, with the absence of a pigmented network and the presence of bluish-gray ovoid nest and arborizing telangiectasias. (C) RCM mosaic image (2.5×2.5 mm) at the level of DEJ shows tumor cell islands (yellow arrows) extending to the papillary dermis, surrounded by dark cleft-like spaces (red arrows) and refractile linear fibrous bundles (asterisk). (D) Individual RCM image (0.5×0.5 mm) at the level of the superficial dermis shows lobulated tumor islands (T) composed of tightly packed, weakly refractile cells with peripheral palisading of nuclei surrounded by moderately refractile stroma (S). (E) Peritumoral dark cleftlike spaces (arrows) are also seen. The RCM image (0.5×0.5 mm) at the level of the superficial dermis shows a dilated blood vessel (arrows) coursing through the tumor (T). (F) On histopathology, the lesion proved to be a nodular BCC.

nodules, islands, cords, or elongated strands of crowded, atypical basaloid cells (Figure 5.3F). The cells have a dark oval nucleus and scant cytoplasm. The tumor aggregates frequently show peripheral palisading of nuclei [11,12].

On RCM, BCCs display tumor islands composed of ill-demarcated cells (Figure 5.3C and 5.3D). In pigmented BCCs, the tumor islands appear bright and are sometimes admixed with dendritic melanocytes. Reactive stromal fibrosis is manifested as thick, bright collagen bundles around the tumor islands (Figure 5.3C). Interestingly, a dark cleft separating the tumor island from the surrounding stroma can sometimes be seen *in vivo*, similar to the cleft seen in BCC around the neoplastic aggregates on histopathology. This dark cleft is probably due to mucin that envelopes tumor islands. Particularly in nonpigmented BCCs, the tumor islands themselves are often not discernible, but their presence can nevertheless be deduced by their appearance as “dark silhouettes” within the bright collagenous stroma. Additional features are the prominent inflammatory infiltrate in the dermis and the increased blood flow in dilated vessels that course *en face* (i.e., parallel to the skin surface) (Figure 5.3E) [13–15]. These blood vessels correlate with the telangiectatic vessels seen on clinical examination of BCC and with the arborizing vessels seen with dermoscopy. The RCM features of BCCs of various histopathologic subtypes of BCC, such as morpheaform BCC, need to be delineated further in the future.

5.3.2 Actinic Keratosis and Squamous Cell Carcinoma

Actinic keratoses (AKs) and squamous cell carcinomas (SCCs) present clinically (i.e., to the naked eye) as erythematous, hyperkeratotic macules, papules, and plaques occurring on sun-damaged skin. Although the clinical diagnosis is usually straightforward, histopathologic evaluation remains the gold standard for diagnosis.

Actinic Keratosis AKs are keratinocytic neoplasms that can develop into invasive SCCs [16]. Dermoscopic findings are often nonspecific [9,17]. Histopathologically, AKs are usually characterized by abnormal keratinocytes that display crowding of nuclei and nuclear atypia, including nuclear enlargement, pleomorphism, and hyperchromasia. There is abnormal maturation of keratinocytes with overlying parakeratosis. The portion of the epidermis traversed by sweat ducts and hair follicles is usually spared and displays orthokeratosis [9].

RCM findings correlate well with routine histopathology [16] and the main features of AKs are nuclear pleomorphism and disorganized spinous and granular layers, resulting in an abnormal or absent honeycomb pattern; hyperkeratosis or parakeratosis; and inflammatory cells, blood vessel dilatation, and solar elastosis in the dermis. Ulrich et al. studied RCM characteristics in 46 AKs compared to normal skin and concluded that architectural disarray at the level of spinous layer (i.e., loss of the honeycomb pattern) and keratinocytic pleomorphism are the best discriminatory features of AKs compared to normal skin, with sensitivity values ranging from 91.2 to 100% and specificity ranging from 95.2 to 100% [18].

Squamous Cell Carcinoma Squamous cell carcinoma (SCC) is the second most common skin malignancy in humans [19]. Clinically, SCC appears as scaly, erythematous papules or plaques, sometimes with a history of bleeding, or as ulcers with an irregular fleshy surface (Figure 5.4A). Dermoscopy may reveal findings such as focal glomerular blood vessels, scale, and hemorrhagic or serous crusting (Figure 5.4B) [20]. Histopathologically, there is a proliferation of abnormal keratinocytes, displaying crowding and pleomorphism of nuclei; dyskeratotic keratinocytes showing abundant eosinophilic cytoplasm as evidence of abnormal, premature cornification; confluent parakeratosis without sparing over hair follicles and sweat ducts. The abnormal keratinocytes may be confined to the full thickness of the epidermis (SCC in situ), sometimes with extension down follicular epithelium, or the proliferation of neoplastic cells may extend into the reticular dermis (invasive SCC) [9,21].

The typical features of SCC may be identified by RCM if hyperkeratosis, which obstructs the penetration depth of imaging (because keratin is highly refractive), is minimal. The use of keratolytic agents to remove the surface scale may facilitate RCM evaluation of hyperkeratotic lesions. The main RCM findings in SCCs are full-thickness architectural disarray (Figure 5.4C) and enlargement and pleomorphism of nuclei of keratinocytes (Figure 5.4D and E). Aggregates of keratinocytes in the dermis may also be seen on occasion and attest to an invasive SCC.

RCM may be limited in the ability to differentiate, with conviction, AKs from SCC, as there is overlap in the RCM features of these entities that span the spectrum of keratinocytic neoplasms; RCM is also limited in evaluation of the dermis for invasive SCC, due to insufficient penetration depth of imaging, particularly in hyperkeratotic lesions. Nevertheless, the epidermal changes in SCC generally involve broader areas and are more pronounced; a complete loss of the honeycomb pattern of the spinous layer (termed *disarranged patter*) is characteristic for SCC [9]. In AKs, the superficial layers of the epidermis may be uninvolved or display an abnormal, yet discernible honeycomb pattern; areas showing epidermal abnormality are less broad than in SCC.

5.3.3 Melanoma

Malignant melanoma is one of the most aggressive skin cancers in humans, and its diagnosis can be challenging even for the best of clinicians (Figure 5.5A, E, and F). Visual inspection and dermoscopic evaluation (Figure 5.5A) allows for a diagnostic accuracy of up to 85% for experienced physicians. The ability to recognize individual melanocytes and to analyze their morphology and distribution provides the basis for using RCM for the in vivo diagnosis of melanoma [6,22–26].

RCM imaging of melanoma reveals enlarged atypical cells with pleomorphic morphology (oval, stellate, or fusiform), coarse branching dendritic processes, and eccentrically placed large dark nuclei. These cells may be found in superficial layers of the epidermis (pagetoid dissemination) and in the dermis (Figure 5.5C

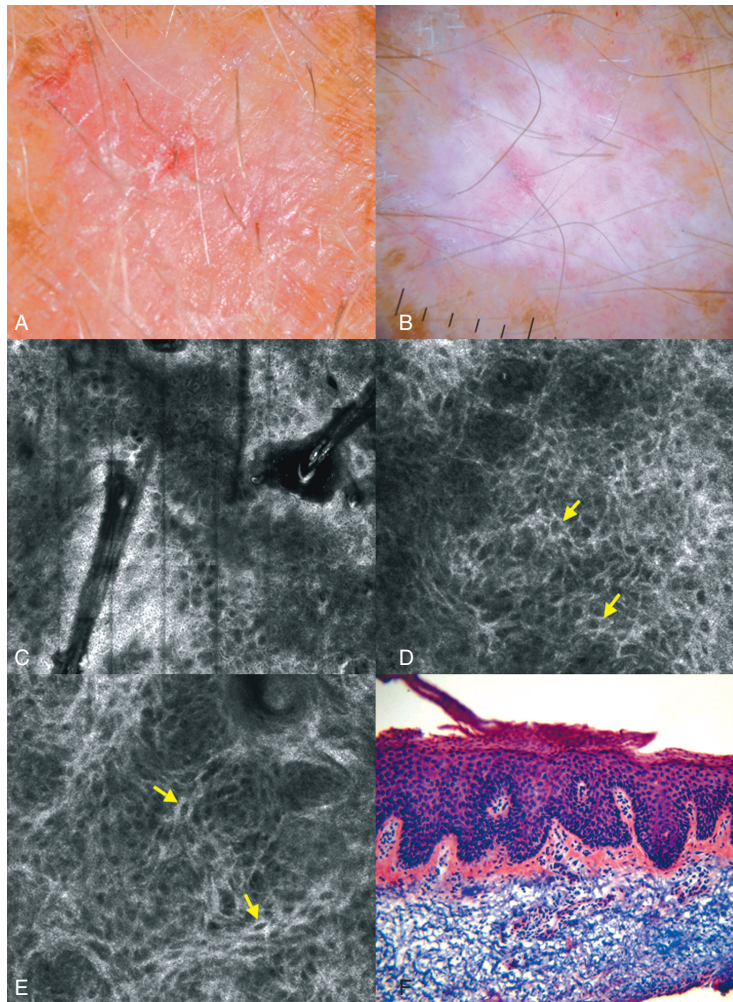


Figure 5.4 (A) Clinical photograph of an erythematous scaly plaque on the forearm. (B) On dermoscopy, this lesion reveals a central scale and diffuse dotted vessels. (C) RCM mosaic image (3.5×3.5 mm) at the level of spinous-granular layers shows areas of an atypical honeycomb pattern. (D,E) Individual RCM images (0.5×0.5 mm) at the level of the spinous-granular layer show an atypical honeycomb pattern composed of large nucleated cells with variability in nuclear size and cellular brightness (arrows), indicating keratinocytic atypia. (F) On histopathology, this proved to be a squamous cell carcinoma in situ. The epidermis shows abnormal crowding of nuclei of keratinocytes (inset).

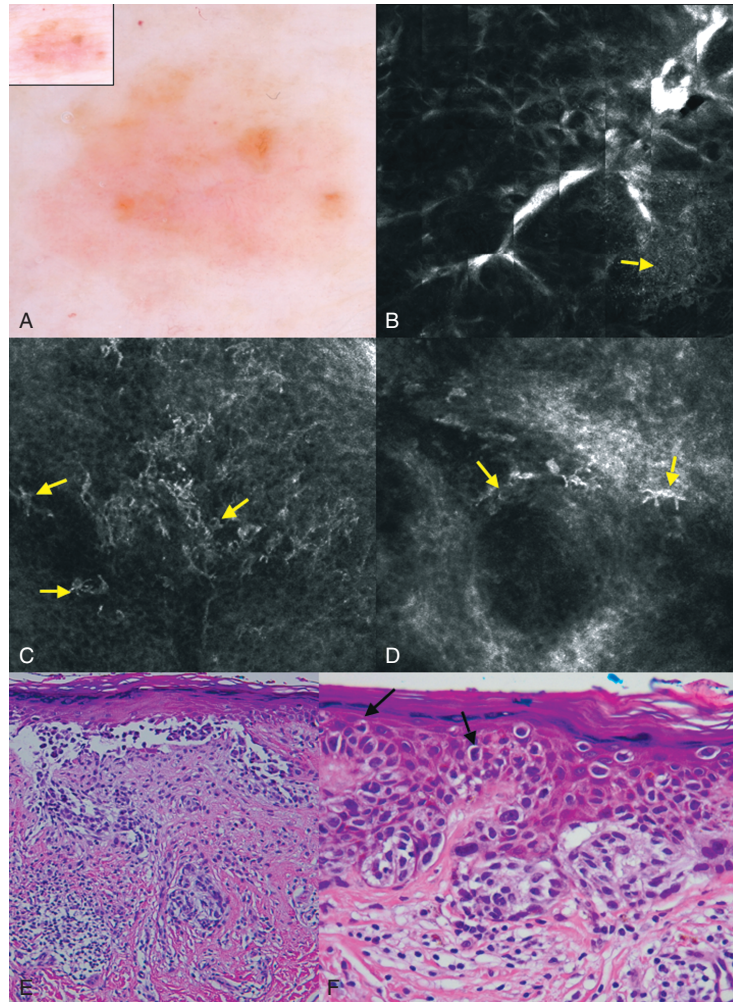


Figure 5.5 (A) This lesion, on the lower back, shows clinically (inset) and dermoscopically a structureless pattern, mostly pink in color with few foci of tan pigmentation and an indistinct border. (B) RCM mosaic image (4×4 mm) at the level of the DEJ shows nonuniform brightness, with a focus that reveals a sheet of cells (arrow). (C,D) Individual RCM images (0.5×0.5 mm) show numerous stellate (dendritic) nucleated cells in the spinous layer (arrows), with partial (C) and complete (D) loss of the normal honeycomb pattern. (E,F) On histopathology, this proved to be an invasive malignant melanoma with an in situ component. Pagetoid cells can be seen in the spinous layer (F, arrows).

and D). It is also common to observe a disruption of the regular honeycomb architectural pattern of the stratum spinosum, indistinct cell borders and bright grainy particles, which probably represent melanin (“melanin dust”), distributed within the epidermis (Figure 5.5B) [26]. The dendrites seen in melanoma appear thickened and bright (Figure 5.5D). Dermal papillae in melanoma may be irregular in size and shape, with ill-defined borders that lack the surrounding ring of bright basal cells (“nonedged papillae”), or may be completely unapparent, due to flattening of the dermal–epidermal junction. Cerebriform clusters or sparse cell nests can also be seen in the dermis on occasion. These structures consist of irregularly bright cell aggregates, with nondemarcated cell borders and pleomorphism, surrounded by melanin dust.

Criteria to distinguish between benign and malignant pigmented lesions are currently in flux. Despite this, RCM images from the DEJ allow for the discrimination between nevi and melanomas with a high degree of certainty [27,28]. The ability of RCM to discriminate nevi from melanoma is based on the evaluation of the lesion’s overall architecture and melanocytic cytomorphology.

A diagnostic algorithm for RCM evaluation of clinically (i.e., to the naked eye) and dermoscopically equivocal melanocytic lesions has recently been proposed by Pellacani et al. [29]. This algorithm has two major and four minor confocal criteria associated with malignancy, with a total score that ranges from zero to eight. Major criteria (scored 2 points each in the diagnostic algorithm) are the presence of nonedged papillae (lack of a ring of bright basal cells around dermal papilla) and the presence of atypical melanocytes (larger than normal melanocytes, abnormal in shape and refractivity) at the basal layer. Minor criteria (scored 1 point each) are the presence of pagetoid cells—round, bright, and nucleated cells (corresponding to melanocytes) within the epidermis above the basal layer; widespread infiltration of pagetoid cells throughout the lesion; cerebriform clusters—confluent aggregates, brainlike in appearance, of low-reflecting cells in the dermis (corresponding to dermal aggregates of abnormal melanocytes in melanoma); and bright nucleated cells within the dermal papilla (corresponding to single melanocytes in the dermis). A score ≥ 3 suggests the diagnosis of melanoma with 97.3% sensitivity and 72.3% specificity [29]. In addition, Gerger et al. found that another important criterion for melanoma diagnosis was border disruption between keratinocytes [30].

The presence of melanocytes in the dermis of a lesion that shows features of melanoma raises suspicion for an invasive melanoma. It is important to mention that detection of melanocytes in the superficial dermis with RCM is limited by effective imaging depth of up to 200 μm , due to a decrease in resolution [31].

5.4 MOSAICING OF EXCISED SKIN EX VIVO

Precise surgical excision of epithelial cancers with minimal damage to the surrounding normal tissue requires accurate determination of the borders of the lesion, which is usually guided by the examination of either frozen or permanent

histology sectioning. A well-established technique is Mohs micrographic surgery, which is commonly used to excise BCCs and SCCs on the face. The excision is performed in stages. After each stage the histopathologic sections of the excised tissue are prepared and examined to determine the extent and borders of the tumor. This, in turn, provides guidance on how to proceed with the subsequent excision, if necessary. The preparation of histology is slow and labor intensive, especially in surgical settings, in which speed and efficiency are important. Frozen histology usually requires minutes to hours and permanent histology may require hours to days. Real-time confocal mosaicing microscopy, combined with clinically useful contrast agents, may help detect the cancers directly in the fresh surgical excisions, at the bedside, while minimizing the need for frozen histology. Since the cancer-to-normal tissue margins are to be detected on the surface or in the superficial layers of the excision, confocal microscopy is very well suited for this application. Rapid examination for cancers at low ($2\times$) magnification, followed by inspection of nuclear morphology at high (10 to $30\times$) magnification may be possible, in a manner that directly mimics the standard for examining Mohs histology sections. Both the patient and surgeon may benefit by saving time, labor, and costs.

Confocal microscopy, at high resolution, is limited to small fields of view of 0.2 to 1 mm. However, stitching together of a two-dimensional matrix of adjacent images, with computer software, allows for the creation and display of mosaics with substantially larger fields of view. These larger fields of view display Mohs surgical excision specimens of size 10 to 20 mm, which is equivalent to viewing with a magnification of $2\times$ [32]. Confocal mosaicing microscopy shows promise in providing pathology-like images of large areas of excised tissue, with low magnification and high resolution, to potentially guide Mohs surgery [7,33]. Confocal mosaicing techniques can map large samples with high resolution. Furthermore, mapping the entire margin enables the rapid detection of residual tumors in surgical excisions. A typical first-stage Mohs excision takes approximately 5 min to image with mosaicing, which is faster than the time required to prepare conventional frozen histology.

Similar to the use of stains in histology, the use of contrast agents increases the detectability of tumors. In reflectance mode, immersion in 1 to 10% acetic acid causes the compaction of chromatin and rapidly enhances nuclear-to-dermis contrast within 0.5 to 5 min, enabling detection of superficial and nodular-type BCC tumors with an accuracy that is comparable to that of routine histology [32,33]. However, infiltrative BCC with small tumor foci remain obscured by the surrounding dermis in reflectance mode imaging.

In fluorescence mode, stains such as acridine orange [7] and toluidine blue [34] yield enhancement of nuclear contrast compared to the background dermal tissue, enabling detection of the smallest micronodular and infiltrative types of BCC tumors. Future work to integrate multiple modes may increase the diagnostic accuracy of confocal mosaicing microscopy to eventually meet or potentially exceed that of frozen histology.

To be able to acquire a two-dimensional matrix of images (to create mosaics) of fresh excised tissue requires that the tissue be flat and properly oriented. For frozen histology, this is usually not a problem, since the tissue is made to conform by freezing the position and orientation in the cryostat so as subsequently to enable proper sectioning. Fresh excision specimens, however, are living, hydrated, supple, and have complex shapes. Thus, to enable mosaicing over large areas, a tissue fixture was engineered for mounting Mohs surgical excisions [7,32,33]. The fixture allows repeatable and accurate control of the flattening, tilt, sag, and stability of the tissue surface to be imaged. The functionality of the tissue fixture mimics the operation of cryostats.

At present, up to 36×36 images may be mosaiced to create a field of view of up to 15×15 mm (Figure 5.6). The large field of view displays the entire excision with resolution and magnification equivalent to $2\times$, which corresponds to that used routinely by Mohs surgeons for examining histology. Submosaics display smaller fields of view at $4\times$ to $10\times$ magnifications with corresponding higher resolution. This corresponds to the Mohs surgeons' use of $4\times$ and $10\times$ magnifications, when necessary, for closer examination of histology.

In a recently completed study, 160 fluorescence submosaics were examined at $4\times$ magnification by two Mohs surgeons who were blinded to the correspondingly frozen histology. Their overall sensitivity was 96.6% and specificity was 89.2%

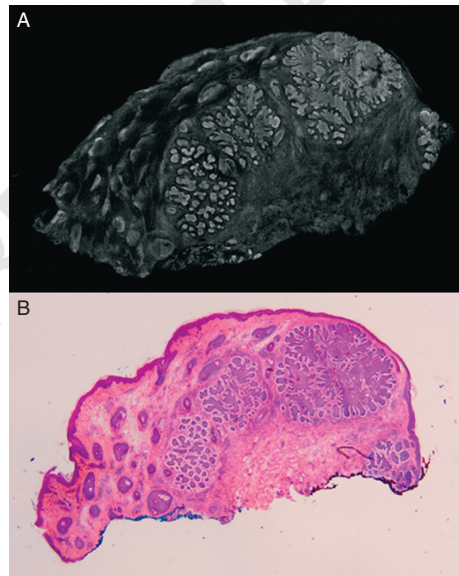


Figure 5.6 (A) Fluorescence confocal mosaic (9 mm wide) of a tissue specimen from Mohs surgery showing nodular and micronodular BCC in the dermis. Fluorescent staining was achieved with immersion of the specimen in 1 mM acridine orange (pH 6.0) in saline solution for 20 s. (B) The corresponding H&E histopathologic micrograph shows excellent correlation with the confocal mosaic.

for detecting the presence and absence, respectively, of all four subtypes (i.e., superficial, nodular, micronodular, and infiltrative) BCC tumors [35].

5.5 INTRAOPERATIVE MAPPING OF SURGICAL MARGINS

Another application of RCM is intraoperative mapping of surgical margins. Malignant neoplasms are often asymmetric, and their margins may not be obvious to the clinical eye. Therefore, these tumors may involve the surgical margins. As mentioned earlier, in Mohs surgery the margins involved are identified by frozen histopathologic sections, and further surgery is undertaken to remove residual tumor, a time-consuming process. However, identifying residual tumor in vivo, directly in the skin surrounding the surgical defect by RCM could allow the surgeon to adjust the surgical margins in real time and would greatly expedite Mohs surgery.

We have begun the research that lays the foundations for intraoperative margin mapping. Challenges for imaging using current technology include adapting the concavity of the surgical defect to the flat plane of RCM imaging, maintaining a sterile wound environment during imaging, and enhancing the visibility of the tumor from the surrounding skin in RCM images. We have found that filling the cavity with a sterile surgical gel and covering with a sterile transparent adhesive address the issues of contour and sterility. The hemostatic agent currently used in skin surgery, aluminum chloride, was found to enhance contrast between nuclei and surrounding dermis, similar to the use of acetic acid ex vivo. Using mosaicing technology of RCM, the clinician can visualize the epidermal, superficial, and deep dermal margins of the surgical defect, and identify residual tumor. Undoubtedly, further miniaturization of the RCM device into a small handheld probe that will fit the surgical defect and discovery of new contrast agent could make intraoperative RCM margin mapping into a practical technique.

5.6 CHALLENGING CASES

In this section we describe two patients who presented at our clinic with skin lesions suspicious for skin cancer, for which RCM enabled the clinician to make the correct diagnosis at the bedside. The first case describes an early diagnosis of melanoma with RCM, enabling timely treatment of this potentially lethal skin cancer. In the second case, the clinician was able to diagnose a much more indolent skin neoplasm, actinic keratosis, and at the same time, to exclude melanoma based on RCM findings.

Case 1

Clinical Presentation A 41-year-old man with a family history of melanoma presented with an enlarging pigmented lesion on the back. He denied pruritus, bleeding, or other complaints. On general skin examination, the patient had multiple pigmented lesions on his torso and limbs. A brown, asymmetrical, slightly

raised lesion, 6 × 4 mm in size, was observed on the midback (Figure 5.7A). Regional lymph nodes were not enlarged on palpation.

Dermoscopic Features The lesion was dark brown and showed a diffuse network that was focally thickened (Figure 5.7B). A peripheral structureless area imparted asymmetry to the lesion. The overall impression was that the lesion is probably a dysplastic nevus, however, the history of change and asymmetric morphology prompted further investigation by RCM.

RCM Features The lesion was scanned using the Vivascope 1500. Three RCM mosaic images (5 × 5 mm field of view) were obtained at the epidermal, DEJ, and dermal levels. Stacks of consecutive individual images (0.5 × 0.5 mm field of view) from the skin surface to the superficial dermis were also obtained at the lesion's center and border. The RCM mosaic at the level of the spinous layer of the epidermis demonstrated heterogeneous reflectivity and the presence of multiple bright cells (Figure 5.7C). The individual RCM images (analogous to higher-magnification examination on histopathology) at the level of the spinous layer showed absence of the normal honeycomb pattern, replaced by sheets of bright round and dendritic nucleated cells (Figure 5.7D). Imaging at the DEJ level revealed widening of the spaces between dermal papillae (corresponding to epidermal rete ridges) and abnormal density of dendritic cells (Figure 5.7E). The RCM examination was suggestive of a melanoma and the lesion was fully excised.

Histopathologic Examination The biopsy revealed junctional proliferation melanocytes as nests and solitary units with few melanocytes scattered in the spinous layer of the epidermis. The papillary dermis showed fibrosis and inflammation. After deliberation and consistent with the RCM findings, the dermatopathologist diagnosed the lesion as an early in situ melanoma (Figure 5.7F).

Case 2

Clinical Presentation A 74-year-old man presented to our clinic with a pigmented lesion on the nose. He did not recall any changes in the lesion over the past five years. On general skin examination, several solar lentigines were seen on the face, suggestive of sun-damaged skin. A brown variegated elliptical 8 × 4 mm lesion was seen on the right side of the nose, below the right eye (Figure 5.8A). No regional lymph nodes were palpable. The differential diagnosis included AK, early SCC, and melanoma.

Dermoscopic Features The lesion was asymmetric with a gray-brown network-like pattern (Figure 5.8B). The clinician was still unable to make a specific diagnosis, based on the dermoscopic findings, and therefore decided to proceed to RCM examination.

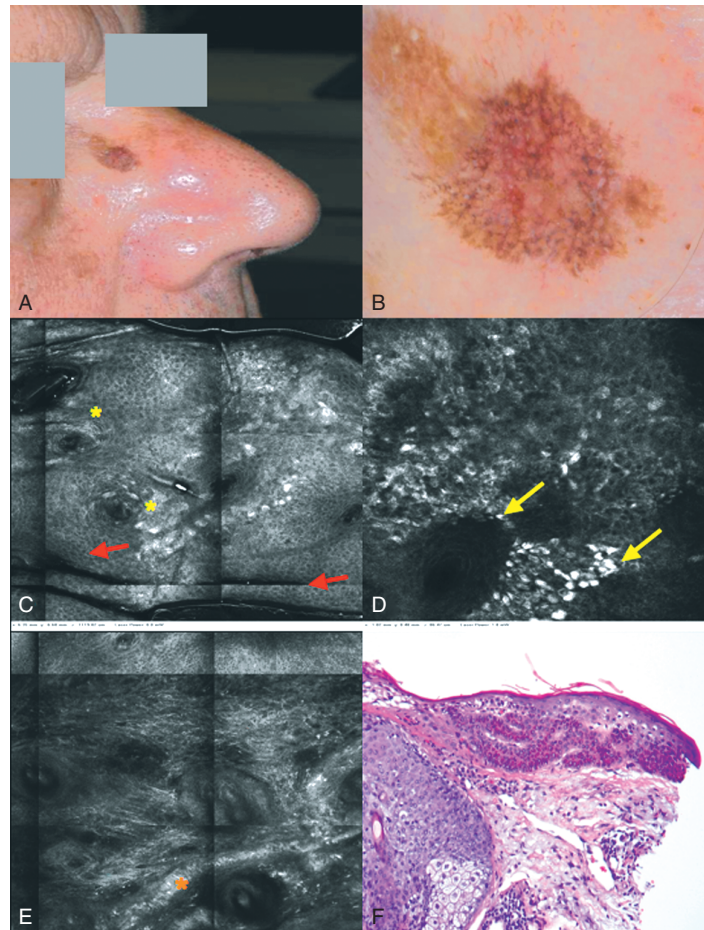


Figure 5.7 (A) Clinical image; (B) dermoscopic image (obtained using nonpolarized contact dermoscopy). (C) At the level of the epidermal spinous layer, the RCM mosaic (a 1.5×1.5 mm field of view is shown) shows heterogeneous reflectivity with sheets of bright cells (yellow arrow) standing out from the background epidermis (red arrows). (D) The RCM individual image (0.5×0.5 mm) at the spinous layer level shows bright nucleated round (yellow asterisks) and dendritic cells (red asterisk). (E) An individual RCM image at the DEJ level shows that the dermal papillae (green arrows) are abnormally separated by widened rete ridges that contain an abnormal density of dendritic nucleated cells (orange asterisks). (F) On histopathology (H&E staining), a nested melanocytic proliferation in widened rete ridges can be seen as well as papillary dermis fibrosis and inflammation. Proliferation of single melanocytes at foci of the DEJ as well as scattered in the spinous layer were also seen. The final diagnosis was an early in situ melanoma.

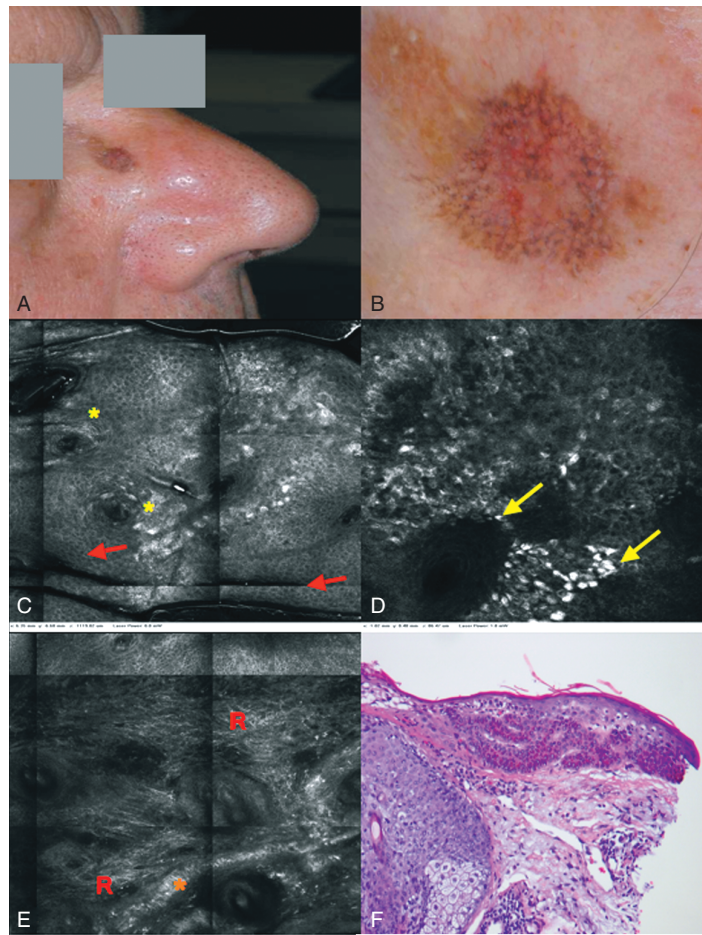


Figure 5.8 (A) Clinical image; (B) dermoscopic image (obtained using nonpolarized contact dermoscopy). (C) The RCM mosaic (2×2 mm field of view is shown), at the level of the epidermal spinous layer, showing heterogeneous reflectivity with mostly typical honeycombed pattern (red arrows) and some atypical areas. The honeycomb pattern at foci is disrupted, showing abnormal bright granularity (yellow asterisks). (D) The RCM individual image (0.5×0.5 mm) at the level of the basal and spinous layers of the epidermis shows bright cells with some variability of size, shape, and refractility (yellow arrows), compatible with atypical pigmented keratinocytes. No dendritic cells or elements are seen. (E) The RCM individual image (0.5×0.5 mm) at the DEJ and superficial dermis level shows elongated pigmented rete ridges (orange asterisk) and abundant reticular collagen (red R), with many small, bright cells (inflammatory cells). (F) On histopathology (H&E staining), a hyperplastic epidermis with elongated, budding rete ridges is seen. The basal keratinocytes are pigmented and show an abnormal crowding of nuclei. The underlying dermis shows solar elastosis, attesting to chronic sun damage. The lesion was diagnosed as pigmented proliferative actinic keratosis with a dense chronic inflammatory infiltrate.

RCM Features Three RCM mosaic images (5×5 mm field of view) were obtained at the epidermal, DEJ, and dermal levels. Stacks of consecutive individual images (0.5×0.5 mm field of view) from the skin surface to the superficial dermis were also obtained. A mosaic imager at the level of the epidermal spinous layer showed areas of a typical honeycomb pattern alternating with areas showing disrupted pattern with heterogeneous reflectivity and scattered bright cells (Figure 5.8C). An atypical honeycomb pattern was seen focally (Figure 5.8D). RCM imaging at the level of the superficial dermis showed abundant reticular collagen and many bright small cells, corresponding to inflammatory cells (Figure 5.8E). No nucleated cells or nests were seen; there were also no dermal tumor islands or “dark silhouettes” to suggest BCC. The focal pleomorphism of keratinocytes, seen as atypical honeycomb, along with lack of pagetoid cellular spread or atypical melanocytes, suggested the diagnosis of AK/early SCC, not melanoma or BCC. A biopsy was performed to rule out an SCC.

Histopathologic Examination The lesion was diagnosed as a pigmented, proliferative actinic keratosis (Figure 5.8F).

These two cases demonstrate the immense potential that RCM presents to the trained clinician as a sensitive and specific bedside diagnostic tool for the early detection of melanoma and nonmelanoma skin cancer. By adhering to a methodical imaging protocol followed by algorithm-driven diagnostic criteria, RCM allows for both an overall architectural evaluation of the epidermis, DEJ, and upper dermis and cytomorphologic evaluation. Cellular atypia and polymorphism, including certain nuclear morphologies, can also be visualized in vivo and assist in diagnosis.

At present, diagnosis with RCM also presents certain challenges. First, the depth of imaging is limited, which hampers evaluation of lesion morphology in the deeper dermis and in hyperkeratotic lesions. Second, cellular resolution is sub-optimal, and in particular, nuclear details which are indispensable to histopathologic evaluation are difficult to visualize with RCM. Third, in vivo imaging precludes the use of chemical dyes, which at times are useful in histopathology to identify cell types with specificity.

Despite these limitations, RCM shows great potential to serve as an adjunct that significantly improves the bedside accuracy of diagnosis of melanocytic lesions. Pellacani et al. [28] and Guitera et al. [27] have shown recently that in the diagnosis of melanoma, RCM imaging and interpretation by experts resulted in comparable sensitivity to dermoscopy (about 90%) while doubling the diagnostic specificity (RCM 70% vs. dermoscopy 32%). The difference in specificity was even more pronounced in favor of RCM in the evaluation of lightly pigmented or pink melanocytic lesions, which often lack specific dermoscopic features. The authors conclude that RCM has added value in the management of melanocytic lesions.

5.7 FUTURE PERSPECTIVES

Reflectance confocal microscopy is an exciting technology with significant promise for clinical utility in dermatology. However, for confocal microscopy to succeed in diverse clinical settings worldwide, the instrumentation must be made smaller, simpler, more robust with repeatable performance, and less expensive. Toward these goals, a handheld confocal microscope (VivaScope 3000) has been developed by Lucid Inc. Alternative simpler designs based on line scanning (instead of the standard point scanning), along with the use of linear array detectors, are being investigated. Such designs, if successful, may eventually reduce the cost of an RCM to less than 20% of its current cost.

Other developments include synergistic multimodal combinations of imaging and spectroscopy. For example, confocal microscopy to visualize nuclear morphology in the epidermis may be combined with optical coherence tomography that shows overall tissue architecture at increased depths in the dermis. Similarly, confocal imaging to observe morphology is being combined with Raman spectroscopy, which provides biochemical information. While the imaging may provide high sensitivity for the detection of cancer, the spectroscopy may provide higher specificity values.

As the translation of RCM from the laboratory into the clinic (i.e., bench to bedside) continues to progress, there are both opportunities and challenges for clinicians and engineers. The key opportunity for the clinician is the ability to observe large volumes of tissue at near-histological resolution in vivo and in real time, and the corresponding challenge is to determine clinical utility and new paradigms. In the short term, the imaging may guide biopsy and lead to intelligent pathology: pathology that is better directed by the subsurface nuclear-level features shown by confocal microscopy. In the longer term, entirely noninvasive screening and diagnosis may be possible. Screening for detection (and prognosis) of early precancers in the epidermis may be a particularly exciting opportunity. The key challenge is image understanding: developing the ability to interpret black-and-white images without the benefit of stains. Image understanding will be crucial for improving sensitivity and specificity (especially, specificity) and may in the long term lead to new paradigms in pathology.

The opportunities and challenges for engineers include the development of very low-cost confocal microscopes, along with telemedicine networks that will enable images to be evaluated rapidly, improved endogenous and exogenous modes of contrast (stains), and multimodal instrumentation aimed at providing clinically relevant sensitivity and specificity values.

Acknowledgments

The development of RCM technology and translational/clinical research was supported primarily by grants from the National Institutes of Health (NCI and NIBIB). Additional funding support was provided by the Whitaker Foundation,

Byrne Fund, Geoffrey Beene Cancer Research Center, and Lucid Inc. We thank Jay Eastman and William Fox for Lucid's support and partnership.

REFERENCES

1. el Gammal, S., et al., Improved resolution of magnetic resonance microscopy in examination of skin tumors, *J. Invest. Dermatol.*, Vol. 106, 1996, pp. 1287–1292.
2. Wezel, J., Optical coherence tomography in dermatology: a review, *Skin Res. Technol.*, Vol. 7, 2001, pp. 1–9.
3. Jemec, G.B., Gniadecka, M., and Ulrich, J., Ultrasound in dermatology: I. High frequency ultrasound, *Eur. J. Dermatol.*, Vol. 6, 2000, pp. 492–497.
4. Corcuff, P., Bertrand, C., and Leveque, J.L., Morphometry of human epidermis in vivo by real-time confocal microscopy, *Arch. Dermatol. Res.*, Vol. 285, No. 8, 2003, pp. 475–481.
5. Rajadhyaksha, M., et al., In Vivo confocal scanning laser microscopy of human skin: melanin provides strong contrast, *J. Invest. Dermatol.*, Vol. 113, No. 3, 1999, pp. 329–303.
6. Pellacani, G., et al., The impact of in vivo reflectance confocal microscopy for the diagnostic accuracy of melanoma and equivocal melanotic lesions, *J. Invest. Dermatol.*, Vol. 127, No. 12, 2007, pp. 2759–2765.
7. Gareau, D.S., et al., Confocal mosaicing microscopy in Mohs skin excisions: feasibility of rapid surgical pathology, *J. Biomed. Opt.*, Vol. 13, 2008, p. 054001.
8. Huzaira, M., et al., Topographic variations in normal skin, as viewed by in vivo reflectance confocal microscopy, *J. Invest. Dermatol.*, Vol. 116, 2001, pp. 846–852.
9. Gonzalez, M.G., and Halpern, A.C., *Reflectance Confocal Microscopy of Cutaneous Tumors: An Atlas with Clinical, Dermoscopic and Histological Correlations*, Informa Healthcare, London, 2008.
10. Rubin, A.I., Chen, E.H., and Ratner, D., Basal-cell carcinoma, *N. Engl. J. Med.*, Vol. 353, 2005, pp. 2262–2269.
11. Carucci, J.L. D., Basal cell carcinoma, in *Fitzpatrick's Dermatology in General Medicine*, I.M. Freedberg, A.Z. Eisen, K. Wolff, K.F. Austen, L.A. Goldsmith, and S.I. Katz (eds.), McGraw-Hill, New York, 2003.
12. Brenn, T.M. P., Tumors of the surface epithelium: basal cell carcinoma, in *Pathology of the Skin with Clinical Correlations*, P.H. McKee, E. Calonje, and S.R. Granter (eds.), Elsevier Mosby, St. Louis, MO, 2005.
13. Gonzalez, S., and Tannous, Z., Real-time, in vivo confocal reflectance microscopy of basal cell carcinoma, *J. Am. Acad. Dermatol.*, Vol. 47, 2002, pp. 869–874.
14. Nori, S., Sensitivity and specificity of reflectance-mode confocal microscopy for in vivo diagnosis of basal cell carcinoma: a multicenter study, *J. Am. Acad. Dermatol.*, Vol. 51, 2004, pp. 923–930.
15. Sauermann, K., Investigation of basal cell carcinoma [correction of *carcinoma*] by confocal laser scanning microscopy in vivo, *Skin Res. Technol.*, Vol. 8, 2002, pp. 141–147.

16. Aghassi, D., Anderson, R.R., and Gonzalez, S., Confocal laser microscopic imaging of actinic keratoses in vivo: a preliminary report, *J. Am. Acad. Dermatol.*, Vol. 43, 2000, pp. 42–48.
17. Zalaudek, I., et al., Dermoscopy of facial nonpigmented actinic keratosis, *Br. J. Dermatol.*, Vol. 155, 2006, pp. 951–956.
18. Ulrich, M., et al., Clinical applicability of in vivo reflectance confocal microscopy for the diagnosis of actinic keratoses, *Dermatol. Surg.*, Vol. 34, No. 5, 2008, pp. 610–619.
19. Marks, R., Rennie, G., and Selwood, T.S., Malignant transformation of solar keratoses to squamous cell carcinoma, *Lancet*, Vol. 1, 1988, pp. 795–797.
20. Zalaudek, I., Dermoscopy features of pigmented squamous cell carcinoma: a case report, *Dermatol. Surg.*, Vol. 30, 2004, pp. 539–540.
21. Rinker, M.H., et al., Histologic variants of squamous cell carcinoma of the skin, *Cancer Control*, Vol. 8, 2001, pp. 354–363.
22. Busam, K.J., et al., Detection of intraepidermal malignant melanoma in vivo by confocal scanning laser microscopy, *Melanoma Res.*, Vol. 12, 2002, pp. 349–355.
23. Busam, K.J., Detection of clinically amelanotic malignant melanoma and assessment of its margins by in vivo confocal scanning laser microscopy, *Arch. Dermatol.*, Vol. 137, 2001, pp. 923–929.
24. Langley, R.G., et al., Confocal scanning laser microscopy of benign and malignant melanocytic skin lesions in vivo, *J. Am. Acad. Dermatol.*, Vol. 45, 2001, pp. 365–376.
25. Gerger, A., et al., Diagnostic applicability of in vivo confocal laser scanning microscopy in melanocytic skin tumors, *J. Invest. Dermatol.*, Vol. 124, 2005, pp. 493–498.
26. Pellacani, G., et al., Microscopic in vivo description of cellular architecture of dermoscopic pigment network in nevi and melanomas, *Arch. Dermatol.*, Vol. 141, 2005, pp. 147–154.
27. Guitera, P., et al., In Vivo reflectance confocal microscopy enhances secondary evaluation of melanocytic lesions, *J. Invest. Dermatol.*, Vol. 129, No. 1, 2009, pp. 131–138.
28. Pellacani, G., et al., The impact of in vivo reflectance confocal microscopy for the diagnostic accuracy of melanoma and equivocal melanocytic lesions, *J. Invest. Dermatol.*, Vol. 127, No. 12, 2007, pp. 2759–2765.
29. Pellacani, G., Cesinaro, A.M., and Seidenari, S., Reflectance-mode confocal microscopy for the in vivo characterization of pagetoid melanocytosis in melanomas and nevi, *J. Invest. Dermatol.*, Vol. 125, 2005, pp. 532–537.
30. Gerger, A., et al., Sensitivity and specificity of confocal laser-scanning microscopy for in vivo diagnosis of malignant skin tumors, *Cancer*, Vol. 107, 2006, pp. 193–200.
31. Curiel-Lewandrowski, C., et al., Use of in vivo confocal microscopy in malignant melanoma: an aid in diagnosis and assessment of surgical and nonsurgical therapeutic approaches, *Arch. Dermatol.*, Vol. 140, 2004, pp. 1127–1132.
32. Patel, Y.G., et al., Confocal reflectance mosaicing of basal cell carcinomas in Mohs surgical skin excisions, *J. Biomed. Opt.*, Vol. 12, No. 3, 2007, p. 034027.
33. Gareau, D.S., Confocal mosaicing microscopy in skin excisions: a demonstration of rapid surgical pathology, *J. Microsc.*, Vol. 233, 2009, pp. 149–159.

REFERENCES

185

34. Al-Arashi, M.Y., Salomatina, E., and Yaroslavsky, A.N., Multimodal confocal microscopy for diagnosing nonmelanoma skin cancers, *Lasers Surg. Med.*, Vol. 39, 2007, pp. 696–705.
35. Karen, J.K., et al., Detection of basal cell carcinomas in Mohs excisions with fluorescence confocal mosaicing microscopy, *Br. J. Dermatol.*, Vol. 160, No. 6, 2009, pp. 1242–1250.

UNCORRECTED PROOFS

UNCORRECTED PROOFS